Shaping neurons: how morphological constraints affect axonal polarity

Sophie Roth[1,2,3,4], Mariano Bisbal[2,3], Jacques Brocard[2,3], Ghislain Bugnicourt[1,2], Yasmina Saoudi[2], Annie Andrieux[2], Sylvie Gory-Fauré[2] and Catherine Villard[1,5]

[1]Institut Néel and Consortium de Recherche pour l'Emergence des Technologies Avancées, CNRS et Université Joseph Fourier, BP 166, F-38042 Grenoble Cedex 9

[2]Institut National de la Santé et de la Recherche Médicale, U836-GIN; Commissariat Energie Atomique, iRTSV-GPC; BP170, 38042 Grenoble, Cedex 9, France

[3]These authors contributed equally to this work

[4]Present address, Amolf Institute, group Bio-assembly and organization, Science Park 104, 1098 XG Amsterdam, The Netherlands

[5]Corresponding author

Abstract

Neuronal differentiation is under the tight control of biochemical and physical information arising from micro-environment. Here, through a panel of poly-L-lysine micropatterns, we wished to assay how external geometrical constraints of neurons may modulate axonal polarization. Constraints applied to either the cell body or to the neurite directions revealed the existence of a differential mechanical tension between the nascent axon and other neurites. Also, we show that centrosome location is not predictive of axonal polarization but responds to the force exerted by the nascent axon. Using curved trajectories for neurite growth inhibited axonal differentiation and prevented formation of multiple axons normally induced by cytochalasin or taxol treatments. Finally we provide evidence that microtubules act as curvature sensors during neuronal differentiation. Thus, biomechanics coupled to physical constraints might be the first level of regulation during neuronal development, primary to biochemical and guidance regulations.

Keywords: Axon | differentiation | centrosome | cell mechanics | micropatterns

Introduction

In vivo, the behavior of cells and tissues is determined by a combination of biochemical and physical signals. Cells exert forces and sense the environment to modulate their fundamental functions such as migration and differentiation. The impact of the

mechanical and geometrical features of the surrounding matrix on the structure and functions of cells has been increasingly documented[1-3]. In neurons, cytomechanics acts at several steps of the developmental program. The balance between proliferation and differentiation of neuronal stem cells is modulated by differential forces[4], new-born neurons are subjected to passive and active mechanical stress that regulates neurite outgrowth and morphogenesis [5], and growth cones pull and stretch neurites[6]. The topology of the environment is crucial during neurodevelopment, as either glial cells or pre-existing axons are physical supports along which neurons migrate or extend axons toward their distant targets[7-10]. During neuronal differentiation, the nascent axons have to sense and to adapt to the complex topologies arising from the crowded environment of developing brain[8]. How physical constraints of the micro-environment affect axonal polarization remained poorly described[11, 12]. It is known, however, that submitting equivalent neurites to external forces allowed the specification of the stretched neurite into an axon, even in already polarized neurons[13]. At the biological level, both neuronal differentiation and the establishment of forces involve cytoskeletal components; axonal specification correlates with cytoskeletal rearrangements, including local dynamic instability of actin and stabilization of microtubules[14]. Also, the crucial contribution of the centrosome as a microtubule-organizing center during axonal specification remains debated. Centrosome location has been reported as a predictor of axonal fate[15, 16], but this assertion was later questioned by both *in vitro* and *in vivo* observations[17, 18].

Here we wished to assay how external geometrical constraints applied to the cell body and/or to the neurites will be sensed and integrated by neurons, how they may contribute to the regulation of the tension developed by neurites during growth, and how they may modulate axonal polarization.

We thus manipulated neuronal shape through non-specific poly-L-lysine-covered micropatterns. By applying geometrical constraints on the cell body we provide evidence that centrosome location is not predictive of axonal polarization; rather, it is determined by axonal location. Then, by varying the orientation of the directions of neurite growth, we show that the neurite that displays the highest tension becomes the axon, suggesting that axonal specification may result from the achievement of the highest mechanical tension. More, we demonstrate that axonal specification of neurites grown on curved lines is inhibited. This inhibitory effect toward axon formation was strong enough to counteract the multiple-axon-promoting action of taxol or cytochalasin. Finally, using cytoskeleton-

related drugs, we found that microtubules are the major players in tension-mediated neuronal polarization.

Results

To assay the effects of physical constraints on neuronal polarization we provided micropatterned substrates to hippocampal neurons in culture, thereby constraining cell bodies and/or neurites. Through photolithography techniques, poly-L-lysine adhesive patterns were engineered on hydrophobic glass coverslips on top of which embryonic hippocampal mouse neurons were plated.

First we designed a control motif, DC, formed with a 20µm-diameter disk for the cell body and three straight lines (L1-L3 directions) built according to a three-fold rotational symmetry (angles=120°, Fig. 1a). After neuron plating we assayed neuronal differentiation at several days of differentiation *in vitro* (DIV). Neurons grown on these micropatterns behaved like randomly cultured neurons[19]; they generated several equivalent neurites (stage 2) and, about 36 hours later, a single neurite underwent rapid elongation and became the axon (stage 3). Accordingly, the early axonal marker tau was found only in the axonal shaft of 3 DIV (Supplementary Fig. 1) and the dendritic marker MAP2 was mainly found in the dendritic compartment of 7 DIV neurons (Supplementary Fig. 7).

The percentage of neurons polarized in each direction (L1-L3) was determined and we found random polarization along L1-L3 (35.8%, 33.2%, and 31.1% along directions L1, L2, and L3, respectively, Fig.1b) as expected from the three-fold symmetry of the DC motif.

Starting from the control DC pattern new patterns were engineered to analyze relations between axonal specification and neuronal internal tension. Geometrical constraints were applied that affected the form and the surface available for cell spreading and the direction and the trajectories available for neuritic outgrowth.

Centrosome location and axonal differentiation in the presence of cell body physical constraints

First, to study the potential role of centrosome location in axonal polarization, we defined a pattern applying geometrical constraints on the cell body. Indeed, an L-shaped

(boomerang) pattern to constrain Hela cells has been shown to result in stereotyped cell shape with a centrosome location at the corner of the motif [20]. Two patterns were designed (Fig. 1a), one with a thick boomerang-like shape (BmS, Supplementary Fig. 2) and another built from a 20µm-diameter disk (DS). Due to its L-shape, the BmS pattern exhibited an asymmetric direction for neurite outgrowth with an angle of 90° between L2 and L3 and of 135° between the other directions (Fig. 1A and Supplementary Fig. 2). This asymmetry for the direction of neurite outgrowth was reproduced in the DS pattern (thus providing a control of cell body constraints for BmS, Supplementary Fig. 2).

Centrosome distribution was analyzed from γ-tubulin immunolabeling in stage 2 undifferentiated neurons (1 DIV). The L-shaped pattern BmS was able to induce centrosome distribution along its symmetry axis (Fig. 1c-d), strikingly reproducing what was observed for HeLa cells[20] and extending to a radically different cellular type the benefits of micropatterns in terms of stereotyped organelle localization. Note that neurons grown over BmS patterns did not display any new actin structures as compared to non-patterned cells; i.e stress fibers were not observed (Supplementary Fig. 3). Instead, microtubule bundles tended to bend along the upper side of the boomerang shape (Fig. 1c). In contrast to BmS, on DS patterns, undifferentiated neurons (stage 2) exhibited a largely central centrosome location (Fig. 1D).

On both patterns, DS and BmS, axonal polarization preferentially occurred along L1 (44.9% and 47.2%, respectively) as compared to random (Fig. 1b) (*, $p < 0.05$) with no significant difference between BmS and DS. Comparing the observations of early centrosome location on DS and BmS patterns (central vs elongated along L1 direction) with the percentage of polarization along L1 clearly indicated that centrosome alignment along the direction of a given neurite did not induce its axonal fate. Thus, the ability of micropatterns to enforce centrosome location along the L1 axis on BmS at stage 2 did not significantly enhance the success rate of polarization along L1 at stage 3.

We then investigated centrosome distribution at stage 3, after axonal polarization. Centrosome distribution quantified on the BmS pattern revealed that, although 64.7% of the centrosomes were still located along the symmetry axis L1 of the pattern, (Z0 area, Supplementary Fig. 4) as compared to 87.5% at stage 2 (***, $p<0.001$), the others spread toward L2 (14.1%) and L3 (20.1%) directions. In the same micropatterns, axonal polarization occurred in each direction with the following ratio: 47.2% for L1, 27.8% for L2, and 23.3% for L3 (Fig. 1B) directions. Thus at stage 3, on BmS patterns, the

percentage of centrosome positions seemed to be associated with polarization success along each direction. These results indicated a probable redistribution of the centrosome toward the actual axon, following axonal specification. To directly address this possibility we analyzed the centrosome location and the position of the axon from the same individual neuron and found, as displayed in Figure 1e, a direct correlation between centrosome and axonal positioning with a systematic alignment of the centrosome along the axonal direction.

Altogether, these results showed that the initial centrosome localization is not the key factor leading to the observed preferential axonal polarization along L1; rather, it is determined by axonal location. To explain the axonal preference along L1 in BmS and DS patterns, we focused on the rotational symmetry breaking in the neuritic directions in these motifs as compared to the DC control pattern. Hence, we used a geometrical approach of the mechanical tensions developed in each patterns by considering that neurites were in mechanical equilibrium[6]. The vectorial analysis of these tensions yielded different values for their modulus along direction L1 (T_{L1}, Fig. 1f), i.e. T_{L1} was higher by a factor of $\sqrt{2}$ on DS and BmS than on DC control pattern. This analysis suggested that the neurite that displayed the highest tension probably became the axon and that intrinsic asymmetry of tensions may be involved during axonal differentiation. In brief, an intrinsic differential of tension was possibly associated with axonal polarization and could trigger a redistribution of the centrosome population toward the basis of the axon.

Effect of neuritic constraints on axonal differentiation

Geometrical constraints were applied to neurite trajectories by imposing curved lines for neuritic outgrowth. By doing so we wished to mimic *in vivo* neuronal path-finding in a crowded environment to determine how the corresponding physical constraints might affect neuronal tensions and ultimately axonal polarization.

Curved lines for neuritic outgrowth prevented axonal polarization

We designed a succession of micropatterns offering a 20µm-diameter disk (D) dedicated to soma adhesion and 2µm-thick lines for neurite outgrowth with four directions (L1-L4) made of one straight (L1) and three curved lines (L2-L4) of increasing curvature. Curved paths were built from full or truncated half circles of variable radius in order to set the half wavelength of the curvatures to the value of 20µm (Supplementary Fig 5 for a summary

of these pattern parameters). Additionally, we designed a control pattern named DW0 and characterized by four straight directions L1-L4 (Fig. 2a).

Analysis of axonal specification from 3 DIV neurons grown over this class of micropatterns showed new neuritic outgrowth figures where neurites seemed to be partially (Fig. 2b, upper panel) or totally torn off their curved adhesive track (Fig. 2b, lower panel), which we termed ``unhookings''. Video-microscopy analysis of neuronal differentiation showed that neurites dynamically, and sometimes reversibly, unhooked from the curved adhesive track in a time scale of minutes (Fig. 2c, see also Supplementary Video). The actual unhookings observed at 3 DIV recapitulated irreversible tearing events that occurred during the first three days in culture. These observations led us to consider the probable forces developed within neurites growing onto curved lines (Fig. 2d). Whenever a neurite undergoes internal tension T, unhooking forces $F\gamma$ depending on the specific angle characteristic of each micropattern will tend to tear it off ($F\gamma = 2T\sin\gamma$, Fig. 2d). Hence, actual unhookings corresponded to neurites whose adhesive forces towards the micropattern were overcome by the unhooking forces when increasing tension developed within neurites. In agreement with the mechanical modelization of Figure 2d, quantification of unhooking events in the different patterns showed that increasing the curvature increased the unhooking events as well, reaching 22.7% of neurons with at least one unhooked neurite on the DW4 micropatterns (Fig. 2e). A possible relationship between unhooking forces and axonal polarization resulted from observations of unhooked neurites. Out of 132 neurons grown over DW4 micropatterns, 30 displayed unhookings (22.7%) unevenly distributed between axonal and non-axonal neurites. Of 67 neurons that polarized along L1, 8 unhookings were observed on the (3x67) neurites growing on L2-L4, thus indicating a low 4.0 % probability of unhooking for non-axonal neurites. In contrast, of 65 neurons with axonal polarization along L2-L4, 18 unhooked axons were counted, indicating a significantly higher 27.7% frequency of unhooked axons ($p < 0.001$). Since these results were obtained for DW4 micropatterns with fixed physical parameters ($\gamma = 90°$, $\kappa = 0.1\mu m^{-1}$), the different probabilities of unhooking suggest that maximal internal tensions differ for axonal versus non-axonal neurites.

Correspondingly, quantification of axonal polarization along each direction showed that axonal polarization along L1 increased with the curvature of the L2-L4 lines (Fig. 2f), reaching 52.3% ($p < 0.001$ as compared to random, i.e. 25% in these four-branch patterns)

on the DW4 pattern, whereas the other axons differentiated uniformly onto L2-L4 (Supplementary Fig. 6). We stress here that curvature influenced the process of axonal differentiation but not the process of axonal growth. Once formed, the axon developed freely over hundreds of microns along either straight or curved paths (Supplementary Fig. 7).

Taken together, these results indicated that curved lines of increasing curvature led to increasing unhooking forces, responsible for more actual unhookings and resulting in better axonal polarization along L1, as if curved lines inhibited axonal polarization.

Last, we established a map of centrosome distribution before and after axonal polarization in the DW4 pattern, and observed again that this organelle was not predictive of axonal fate (Supplementary Fig. 8). A mainly central location at stage 2 turned into a reinforcement of centrosome positioning along the preferential axonal direction L1 at stage 3. Moreover, a strict correlation between centrosome localization and axonal direction was again observed.

Curved lines conflicted multiple-axon-promoting effect of cytoskeleton drugs

We further investigated the inhibitory role of curved lines toward axonal polarization by performing experiments using pharmacological compounds known to promote the formation of multiple axons (MA) in hippocampal neurons grown on flat unconstrained substrates[21, 22]. Neurons grown on DW0 control pattern were treated either with cytochalasin (CD, 0.5 μM), taxol (3 nM), or vehicle. At 2 DIV, the proportion of MA neurons was similar to that reported in the literature, i.e. 78.6% and 73.3% MA neurons in the presence of cytochalasin D and taxol, respectively, while virtually none (1.7%) were observed in sham conditions (Fig. 3A).

We then assayed the ability of neurons to develop MA when grown on DW4 patterns whose curved lines inhibited axonal specification the most. In sham conditions, only few MA neurons were detected (1.8%); in the presence of cytochalasin D or taxol, MA neurons were still observed but in significantly smaller proportions than for DW0 (32.0% versus 78.6%, $p < 0.001$ and 25.7% versus 73.3%, $p < 0.001$ for cytochalasin D and taxol respectively) (Fig. 3 A). These results indicated that curved lines displayed a strong axon-inhibiting effect that opposed the multi-axon-promoting action of the drugs.

Microtubules support curvature-mediated inhibition of axonal polarization

The inhibition of axon specification on curved lines most probably involved cytoskeletal relays in neurons. To investigate the involvement of cytoskeleton elements in the inhibitory role of curvature toward axonal polarization, we analyzed axonal preference along L1 from experiments performed in the presence of cytoskeletal-targeted drugs: cytochalasin (actin destabilizer), taxol (microtubule stabilizer), or nocodazole (microtubule destabilizer).

Neurons grown on DW4 patterns were treated with each drug and axonal polarization was measured in neurons displaying a unique axon (Fig. 3b). After nocodazole treatment, as compared to sham conditions, axonal polarization toward L1 was significantly reduced (37.7% versus 50.5%, $p < 0.05$), indicating that microtubule integrity was crucial for the inhibitory effect of curved lines toward axonal polarization. Cytochalasin and taxol induced the formation of multiple axons and this effect needed to be taken into account: after the differentiation of a first axon, neurons will try to develop a second axon and will unequally succeed to do so whether they have developed the first axon on the straight line L1 or along any of the curved lines L2-L4. Thus, the probability of remaining a neuron with a unique axon will differ according to the position of the first axon. We developed a simple probabilistic model of successful axon specification along straight or curved lines to predict expected values of polarization along L1 in the presence of the multiple-axon-promoting drugs (Supplementary Text). We then compared the predicted values of axonal polarization along L1 with the measured values. In the presence of cytochalasin D, the predicted value of polarized neurons in direction L1 was 59.0% and in agreement the measured value was 55.8%. In contrast, in the presence of taxol the predicted value of polarized neurons in direction L1 was 58.4% and the measured value of 47.7% was significantly lower ($p < 0.05$).

Altogether these results demonstrated that cytoskeletal elements were differently involved in the inhibitory ability of curved lines to induce axonal polarization. Actin integrity seemed dispensable for the inhibition of axonal polarization by curved lines. In contrast, more neurites grown along curved lines became axons in the presence of taxol or nocodazole i.e. curved lines' capacity to inhibit axonal polarization was decreased in the presence of MT-targeting drugs.

Discussion

Neuronal polarization is sensitive to external physical constraints

Neuronal differentiation *in vivo* and axonal specification are both under the control of a large number of parameters including adhesion[23, 24] to the extra-cellular matrix, complex responses to guidance molecules[8], and physical constraints[11, 12]. In this study, we especially analyzed the role of specific physical parameters on axonal specification. We developed a simplified protocol in which neurons were plated on top of geometrically constrained micropatterns in a defined cell culture medium. By doing so, we provide evidence that neuronal polarization was indeed sensitive to external constraints such as curved trajectories for neuritic outgrowth. Our results indicate that axon polarization was favored along straight lines; such a scenario might be used *in vivo* by newborn neurons extending their nascent axon along a pre-existing straight direction belonging to a neighbor neuron. Indeed, hippocampal granular neurons extend and fasciculate their axons in the same direction as dentate gyrus neurons, which extend axons to form the mossy fiber bundle[25].

Geometrical constraints revealed internal neuritic tension

The involvement of forces during neuronal differentiation was first described for the growth cone of chick sensory neurons and PC12 cells that pulled onto neurites[6, 26]. Mimicking such forces by mechanically pulling a neurite with a micropipette even caused its active growth[26], with constant parameters dependent on intact actin and microtubular networks[27, 28]. Similar experiments with rodent hippocampal neurons unambiguously demonstrated that pulling a neurite could change it into an axon[13]. Finally, identification of low velocity transport independent from the growth cone[29] and observations of axonal stretching from fixed reference points in chick sensory neurons[30] confirmed that internal neuritic tensions may act in living neurons. Our work extends these observations by revealing endogenous neuritic tension in mouse hippocampal neurons grown on micropatterns. In our system, neurons grown over curved lines displayed figures of unhooking formed by neurites progressively detaching from the curved lines they were growing on. This observation led us to consider that individual neurites were submitted to a fine balance of forces, $F_{adhesion}$ and F_{unhook}, the latter depending on the curvature of its substrate. Recent modeling of chick sensory neurons estimated the friction coefficient relative to adhesion to be about 9600 $N.s.m^{-2}$ [31]. Such adhesion along a full curved line of the DW4 motif (area = 62.8μm^2 for γ= 90°, see Fig. S4) would correspond to a force

$F_{adhesion}$ = 1-10 nN to detach in 1-10 min (Fig. 3 D and supplementary video 1). Interestingly, this value of 1-10 nN is of the same order of magnitude as estimations of resting tension in neurites of PC12 cells (1 nN) or Drosophila neurons (4 nN) and of tension needed to differentiate neurites of rat hippocampal neurons into axons (0.4-1 nN)[30, 32, 33].

A differential in internal neuritic tensions may be involved in axonal polarization

The angular orientation applied to straight neuritic directions seemed to be involved in axonal polarization preference, suggesting asymmetric internal tensions during axonal differentiation and leading us to propose that the neurite that expressed the highest tension probably became the axon. Then, the simple mechanical model displayed in Fig. 2D suggested that neuritic tension may be causal in the unhooking phenomenon revealed in neurons grown over the DW class of micropatterns. When unhooking occurred, we very often observed a pause in growth cone advance and even neurite retraction (Fig. 2C, black arrowhead). Such events could result from a collapse of the initially stretched neurite by the disruption of its adhesive contacts with the PLL curved stripe[31]. Therefore, unhooking, by actively reducing neuritic tension, could participate in the inhibition of axonal polarization on curved lines by introducing a differential of tension between neurites. That axons were dominant within the unhooked neurite population seems, however, not in favor of this hypothesis. But, causal or not, the unhooking phenomena reinforced our finding that axons tend to develop a greater tension than other neurites.

Centrosome positioning is not predictive of axonal polarization but responds to neuritic tension

Our results showed that geometrical constraints imposed by patterns to the soma were responsible for centrosome localization at stage 2, a mainly central location if we provided a circular area for soma adhesion (DS pattern) and a localization along the pattern symmetry axis if a boomerang shape was available for the cell body (BmS pattern). Besides, a closer look into the precise centrosome repartition in the DW4 pattern showed that they preferentially distributed in the lower left quadrant at stage 2 (Supplementary Fig 8). Interestingly, the vectorial sum of the neuritic tensions developed in this pattern (determined as in Fig. 1F, but with the assumption of equal modulus arising from the present undifferentiated state), yielded a resultant directed down and leftward (Fig S8).

The major influence of the adhesion area provided to soma on the centrosome distribution at stage 2 can be thus modulated by neurite allocation around the soma, in other terms by neuritic forces.

The localization of centrosome at stage 2 did not seem to be predictive of axonal polarization, as BmS and DS pattern resulted in the same polarization ability, and as a significant axonal rate of polarization along L1 was further observed in DW4 despite the mainly central centrosome localization imposed by this pattern at stage 2. The centrosome has been reported to be highly motile during axonal differentiation[34, 35] and accordingly we found that centrosome distribution changed between stage 2 and stage 3, being clearly aligned along the chosen axonal direction at stage 3. The sensitivity of centrosome positioning to neuritic forces could be further expressed in the course of axonal polarization. At the end of stage 2, one neurite will take precedence over the others and develop a relatively higher force, thus reorienting the centrosome. This centrosome displacement may in turn stabilize the axonal nature of this highly mechanically active and tensed neurite.

Curvature-mediated inhibition of axonal polarization relies on MT cytoskeleton

No change of axonal preference toward the straight direction L1 was observed in the presence of cytochalasin D, indicating that the molecular support of curvature-mediated inhibition of axonal polarization was not strongly affected when the actin network was perturbed. In contrast, treatment with taxol or nocodazole induced less L1 preference than expected from the observations made in the presence of the vehicle. Both drugs are known to affect the microtubule network but their effect strongly depends on the concentrations used in experiments. Low doses of taxol (below 10 nM) affect microtubule dynamics (growing and shortening events at the ends of microtubules) without inducing massive microtubule stabilization and without increasing the microtubule mass[14, 36, 37] and similarly low doses of nocodazole affect the dynamics of microtubule without depolymerization[38]. In our study we used such low doses of both taxol and nocodazole to affect microtubule dynamics and observed decreased axonal preference toward L1. Given the unhooking figures observed and the vectorial analysis of forces (Fig. 1), it seems that expression of forces mainly occurred in the axonal shaft. We can speculate that microtubule dynamics in the axonal shaft are linked with neuritic tension: the perturbation of microtubule dynamics will affect the mean size of individual MTs within the axonal shaft, allowing them for

more or less bending along curved lines. Interestingly, a recent study using rat dorsal root ganglion neurons grown over propylene tubular surfaces demonstrated that curvature *per se* could be used to control the direction of spontaneous neuritic growth[39]. Neuritic outgrowth was inhibited by the curvature of the tubes when it reached values > $0.05\mu m^{-1}$, much similar to the curvature of DW4 curved lines ($0.1\mu m^{-1}$ when $\gamma = 90°$). Using these values, the authors estimated neuritic bending stiffness and indicated that it was compatible with that of bundled MTs[39]. These data, in addition to our results showing that microtubule integrity and dynamics were necessary for axonal polarization, support the hypothesis that MT may be curvature sensors during neuronal differentiation.

Conclusion

Altogether our results strongly indicate that mechanical tensions at work within neurites can be modulated by the topology of the environment and that neurites will only differentiate into axons under conditions allowing for the highest tension. Mechanical forces are probably causal in axonal polarization and in related events like centrosome positioning along the direction of the axon. There is much work left to understand the molecular cascades connecting the forces to the biological phenomena they are involved in.

Materials and Methods

Micro-pattern fabrication Poly-L-lysine patterns were transferred on glass substrates silanized with 3GPS[40] using UV classical photolithography steps, including Shipley S1805 photoresist spinning (4000 rpm, 0.5µm thickness, 115°C annealing step for 1 min), insulation through a mask, development (Microposit concentrate 1:1, Shipley), PLL deposition (1mg/ml one night), and lift-off using an ultra-sound ethanol bath.

Neuron culture and labeling Mouse hippocampal neurons were prepared as previously described[41] and plated at a concentration of 10,000-20,000 cells/cm^2. For centrosome staining, neurons were fixed and permeabilized for 30 min in 3.7% formaldehyde/0.5% glutaraldehyde/0.1% triton X100. For Ankyrin G immunostaining 6-7 days in vitro (DIV), neurons were fixed for 6 min in methanol (-20°C). Primary antibodies (mouse mAbs against Ankyrin G (Santa Cruz); Tau (clone tau-1, Millipore); MAP2 (clone AP-20,

Sigma); rat mAb against tubulin (cloneYL1/2), and rabbit γ tubulin (M. Bornens, Institut Curie, Paris, France). Secondary antibodies were Alexa488 or Cy3 coupled (Molecular Probes, USA). Isolated neurons were analyzed with an inverted microscope Axioskop 50 (Carl Zeiss, Inc.) controlled by Metaview software (MDS Analytical Technologies) using a 40 x and 63 x oil-immersion objective. Images were digitized using a Coolsnap ES camera (Roper Scientific).

Centriole analysis Image sortings were performed using Labview vision software (National Instrument) and a semi-automatic interface that positioned the datum lines associated with each pattern. The two centrioles were visible in more than 85% of cases and were then pointed separately. When indistinguishable, the unique fluorescent point counted for two centrioles. Density maps of centriole positions were made by a custom-made Matlab program using an algorithm for smoothing of two-dimensional histograms[42]. The centriole distribution according to ROIs was assessed using programs in the free Octave language, administered by the GNU General Public License.

Statistics All percentage comparisons were performed using χ^2 tests as implemented in Prism 4.0 (GraphPad Software, La Jolla, USA).

Acknowledgments

This work was funded by the ANR 'NeuroFETs' ANR-07-PCVI-0007 and by the Nanosciences foundation (Grenoble). The authors thank A. Schweitzer and N. Collomb for excellent technical support, E. Denarier, I Arnal for helpful discussions and critically reading the manuscript, R. Peyroux for helpful discussions about cytomechanics, and M. Bornens for providing the rabbit γ tubulin antibody.

Legend figures

Figure 1: Effect of soma constraints on centrosome position and axonal polarization

(a) Design of patterns DC, DS, and BmS; L1-L3 directions are indicated.

(b) Results of axonal polarization, i.e percentages of 3 DIV neurons with their axon along L1-L3 directions (n= 267, 176, and 194 for the DS, BmS, and DC patterns, respectively). Blue dotted lines: random distribution. *, $p<0.05$; ***, $p<0.001$.

(c) Microtubule labeling (green), highlighting the different organizations of microtubules in DC, DS, and BmS patterns. Nuclei (blue) and centrioles (red) stained with antibodies against γ tubulin. Red arrows point to the centrioles.

(d) Superimposition of centriole scatter plots and density maps on the corresponding pattern (n=154, 168, and 160 for the DC, DS, and BmS patterns, respectively). Neurite growth directions are indicated.

(e) Correlation of centriole positioning (red dots) and axonal localization in the BmS pattern. (n= 31, 12, and 20 for the L1, L2, and L3 directions, respectively).

(f) Neuronal outgrowths represented by polygons of forces in the DC (top) and BmS/DS (bottom) pattern. Each vectorial representation is displayed again on the left, showing the magnitude of the tensions (multiple of T, the tension exerted along the L2-L3 directions) exerted along L1 under the hypothesis of an equilibrium mechanical state at the cell level.

Figure 2: Influence of neurite curvature on axonal polarization

(a) DW4-set of patterns of increasing curvature along directions L2-L4; Scale bars, 20µm.

(b) Partial and complete unhookings observed on fixed cells (microtubules: green, F-actin: red). White arrows point to partial unhooking, characterized by a displaced neuritic shaft still attached to the substrate by a large lamellipodium. The yellow arrow indicates complete unhooking characterized by a high density of MTs crossing the pattern arch and remaining entities strictly following the curved adhesive line. Scale bar, 10µm.

(c) Time-lapse experiment (indicated in minutes, with t_0, taken 30 hours after plating) of a neurite developing on a DW4 pattern showing partial unhooking (white arrow). The black arrowhead points to the neurite tip and the green dashed lines in the upper panels mark the position of the adhesive pattern. Scale bars, 20µm. Refer to supplemental Movie 1 for the original time-lapse sequence.

(d) Physical modeling of a curved neurite (in red) as an elastic wire under tension T. Curvature is reflected by the angle γ (see text), and $F\gamma = 2\ T \sin \gamma$ (black arrow) is the force experienced by the elastic wire.

(e) Number of unhookings plotted from neurons grown over DW0 (0 %), DW4-1 (6 %), DW4-1 (8 %), DW4-3 (13.7 %), and DW4 (26.5 %) patterns. (n = 117, 129, 128, 132, and 132, respectively).

(f) Preferential axonal specification along the straight direction L1 were plotted from 3 DIV neurons plated over DW0 (24.4%), DW4-1 (32.6%), DW4-1 (34.7%), DW4-3 (45.5%), and DW4 (52.3%) patterns. (n = 131, 285, 225, 330, and 216, respectively). ***, significantly different from random, $p<0.001$.

Figure 3 Combined actions of drugs and micropatterns on axonal polarization

(a) Percentages of multiple axon (MA) neurons grown over DW0 or DW4 micropatterns, in sham conditions or in the presence of cytochalasin D (0.5 μM) or taxol (3 nM); (sham n=117; CD, n=112; Tx, n=150 for DW0 and sham n=109; CD, n=153; Tx, n=319 for DW4). ***, significantly different from both DW0, $p < 0.001$.

(b) Axonal preference along L1 for neurons grown on DW4 micropatterns, in the presence of DMSO, nocodazole (Nz); cytochalasin (CD) or taxol (Tx) (n = 107, 146, 104, and 237 neurons with a unique axon, respectively). Blue dotted lines represent the predicted preference along L1 in the presence of CD or Tx as determined with the probabilistic model (Supplementary Text). *, significantly different from the expected distribution, $p < 0.05$.

References

1. Mammoto, T. & Ingber, D.E. Mechanical control of tissue and organ development. *Development (Cambridge, England)* **137**, 1407-1420 (2010).
2. Vogel, V. & Sheetz, M.P. Cell fate regulation by coupling mechanical cycles to biochemical signaling pathways. *Current opinion in cell biology* **21**, 38-46 (2009).
3. Dalby, M.J. Topographically induced direct cell mechanotransduction. *Medical engineering & physics* **27**, 730-742 (2005).
4. Shi, P., Shen, K., Ghassemi, S., Hone, J. & Kam, L.C. Dynamic Force Generation by Neural Stem Cells. *Cell Mol Bioeng* **2**, 464-474 (2009).
5. Van Essen, D.C. A tension-based theory of morphogenesis and compact wiring in the central nervous system. *Nature* **385**, 313-318 (1997).
6. Bray, D. Mechanical tension produced by nerve cells in tissue culture. *Journal of cell science* **37**, 391-410 (1979).
7. Nishio, T. Axonal regeneration and neural network reconstruction in mammalian CNS. *J Neurol* **256 Suppl 3**, 306-309 (2009).
8. Chilton, J.K. Molecular mechanisms of axon guidance. *Developmental biology* **292**, 13-24 (2006).
9. Steinbach, K. & Schlosshauer, B. Regulatory cell interactions between retinal ganglion cells and radial glia during axonal and dendritic outgrowth. *Microscopy research and technique* **48**, 12-24 (2000).
10. Ribak, C.E. & Shapiro, L.A. Dendritic development of newly generated neurons in the adult brain. *Brain Res Rev* **55**, 390-394 (2007).

11. Jang, K.J.*, et al.* Two distinct filopodia populations at the growth cone allow to sense nanotopographical extracellular matrix cues to guide neurite outgrowth. *PLoS ONE* **5**, e15966 (2010).
12. Francisco, H., Yellen, B.B., Halverson, D.S., Friedman, G. & Gallo, G. Regulation of axon guidance and extension by three-dimensional constraints. *Biomaterials* **28**, 3398-3407 (2007).
13. Lamoureux, P., Ruthel, G., Buxbaum, R.E. & Heidemann, S.R. Mechanical tension can specify axonal fate in hippocampal neurons. *J Cell Biol* **159**, 499-508 (2002).
14. Witte, H. & Bradke, F. The role of the cytoskeleton during neuronal polarization. *Current opinion in neurobiology* **18**, 479-487 (2008).
15. Zmuda, J.F. & Rivas, R.J. The Golgi apparatus and the centrosome are localized to the sites of newly emerging axons in cerebellar granule neurons in vitro. *Cell motility and the cytoskeleton* **41**, 18-38 (1998).
16. de Anda, F.C.*, et al.* Centrosome localization determines neuronal polarity. *Nature* **436**, 704-708 (2005).
17. Barnes, A.P. & Polleux, F. Establishment of axon-dendrite polarity in developing neurons. *Annual review of neuroscience* **32**, 347-381 (2009).
18. Zolessi, F.R., Poggi, L., Wilkinson, C.J., Chien, C.B. & Harris, W.A. Polarization and orientation of retinal ganglion cells in vivo. *Neural development* **1**, 2 (2006).
19. Dotti, C.G., Sullivan, C.A. & Banker, G.A. The establishment of polarity by hippocampal neurons in culture. *J Neurosci* **8**, 1454-1468 (1988).
20. Thery, M.*, et al.* The extracellular matrix guides the orientation of the cell division axis. *Nat Cell Biol* **7**, 947-953 (2005).
21. Witte, H. & Bradke, F. The role of the cytoskeleton during neuronal polarization. *Curr Opin Neurobiol* **18**, 479-487 (2008).
22. Bradke, F. & Dotti, C.G. Establishment of neuronal polarity: lessons from cultured hippocampal neurons. *Curr Opin Neurobiol* **10**, 574-581 (2000).
23. Bard, L.*, et al.* A molecular clutch between the actin flow and N-cadherin adhesions drives growth cone migration. *J Neurosci* **28**, 5879-5890 (2008).
24. Dequidt, C.*, et al.* Fast turnover of L1 adhesions in neuronal growth cones involving both surface diffusion and exo/endocytosis of L1 molecules. *Molecular biology of the cell* **18**, 3131-3143 (2007).
25. Blaabjerg, M. & Zimmer, J. The dentate mossy fibers: structural organization, development and plasticity. *Prog Brain Res* **163**, 85-107 (2007).
26. Bray, D. Axonal growth in response to experimentally applied mechanical tension. *Dev Biol* **102**, 379-389 (1984).
27. Dennerll, T.J., Lamoureux, P., Buxbaum, R.E. & Heidemann, S.R. The cytomechanics of axonal elongation and retraction. *J Cell Biol* **109**, 3073-3083 (1989).
28. Dennerll, T.J., Joshi, H.C., Steel, V.L., Buxbaum, R.E. & Heidemann, S.R. Tension and compression in the cytoskeleton of PC-12 neurites. II: Quantitative measurements. *J Cell Biol* **107**, 665-674 (1988).
29. Miller, K.E. & Sheetz, M.P. Direct evidence for coherent low velocity axonal transport of mitochondria. *J Cell Biol* **173**, 373-381 (2006).
30. Lamoureux, P., Heidemann, S.R., Martzke, N.R. & Miller, K.E. Growth and elongation within and along the axon. *Dev Neurobiol* **70**, 135-149 (2010).
31. O'Toole, M., Lamoureux, P. & Miller, K.E. A physical model of axonal elongation: force, viscosity, and adhesions govern the mode of outgrowth. *Biophysical journal* **94**, 2610-2620 (2008).

32. Rajagopalan, J., Tofangchi, A. & MT, A.S. Drosophila neurons actively regulate axonal tension in vivo. *Biophysical journal* **99**, 3208-3215 (2010).
33. Bernal, R., Pullarkat, P.A. & Melo, F. Mechanical properties of axons. *Physical review letters* **99**, 018301 (2007).
34. de Anda, F.C., Meletis, K., Ge, X., Rei, D. & Tsai, L.H. Centrosome motility is essential for initial axon formation in the neocortex. *J Neurosci* **30**, 10391-10406 (2010).
35. Calderon de Anda, F., Gartner, A., Tsai, L.H. & Dotti, C.G. Pyramidal neuron polarity axis is defined at the bipolar stage. *J Cell Sci* **121**, 178-185 (2008).
36. Derry, W.B., Wilson, L. & Jordan, M.A. Substoichiometric binding of taxol suppresses microtubule dynamics. *Biochemistry* **34**, 2203-2211 (1995).
37. Jordan, M.A., Toso, R.J., Thrower, D. & Wilson, L. Mechanism of mitotic block and inhibition of cell proliferation by taxol at low concentrations. *Proceedings of the National Academy of Sciences of the United States of America* **90**, 9552-9556 (1993).
38. Jordan, M.A., Thrower, D. & Wilson, L. Effects of vinblastine, podophyllotoxin and nocodazole on mitotic spindles. Implications for the role of microtubule dynamics in mitosis. *Journal of cell science* **102 (Pt 3)**, 401-416 (1992).
39. Smeal, R.M., Rabbitt, R., Biran, R. & Tresco, P.A. Substrate curvature influences the direction of nerve outgrowth. *Ann Biomed Eng* **33**, 376-382 (2005).
40. Nam, Y., Branch, D.W. & Wheeler, B.C. Epoxy-silane linking of biomolecules is simple and effective for patterning neuronal cultures. *Biosens Bioelectron* **22**, 589-597 (2006).
41. Peris, L*., et al.* Motor-dependent microtubule disassembly driven by tubulin tyrosination. *The Journal of cell biology* **185**, 1159-1166 (2009).
42. Eilers, P.H. & Goeman, J.J. Enhancing scatterplots with smoothed densities. *Bioinformatics (Oxford, England)* **20**, 623-628 (2004).

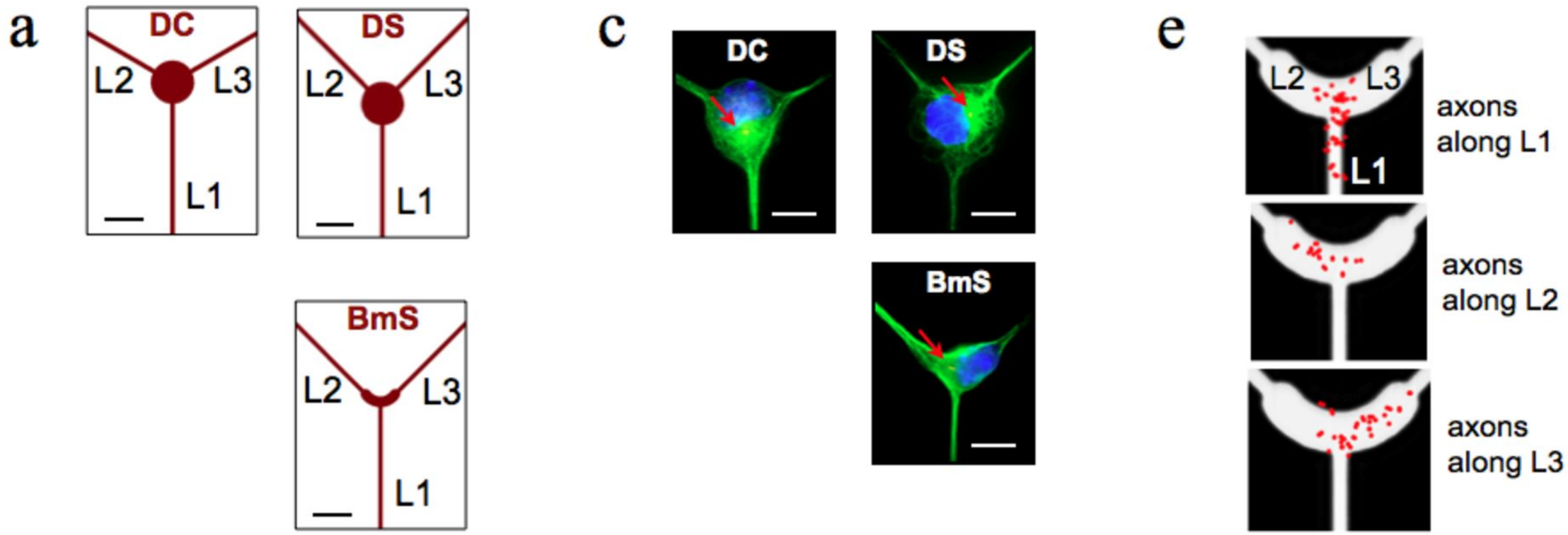

figure-1 (Villard)

a

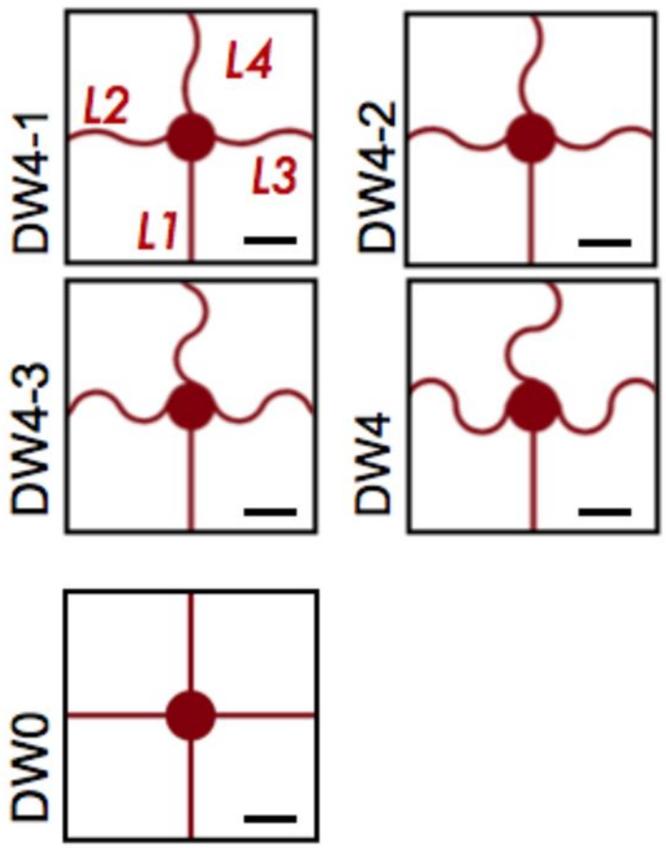

b

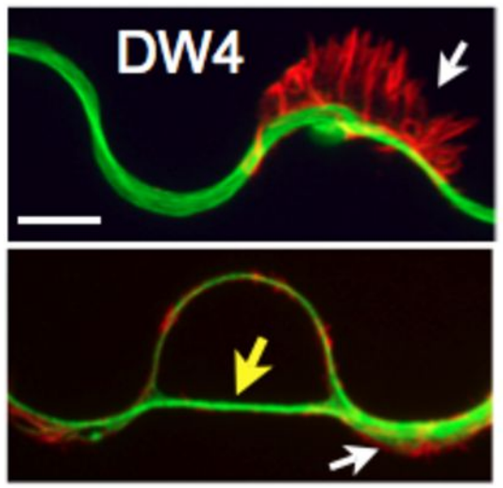

c

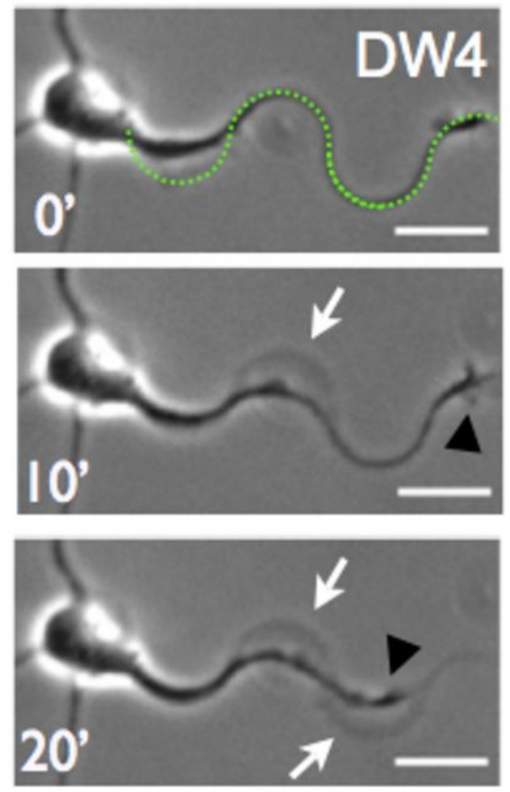

d

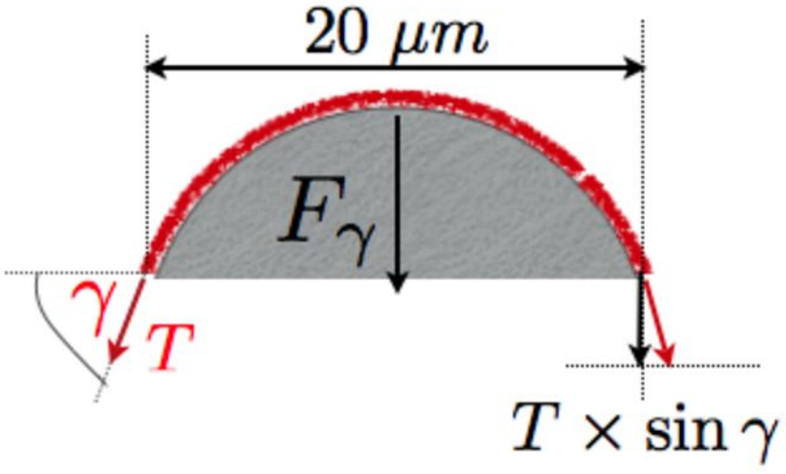

e

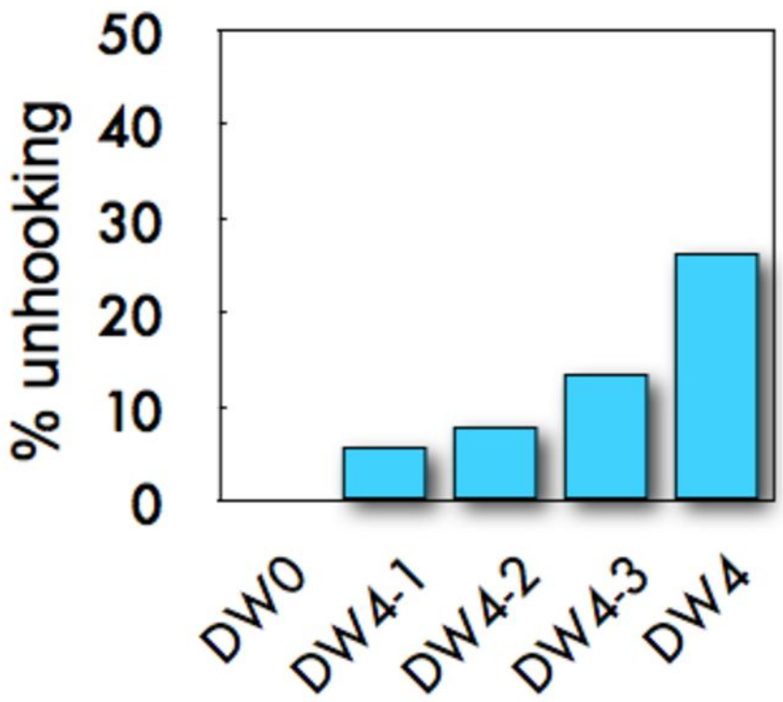

f

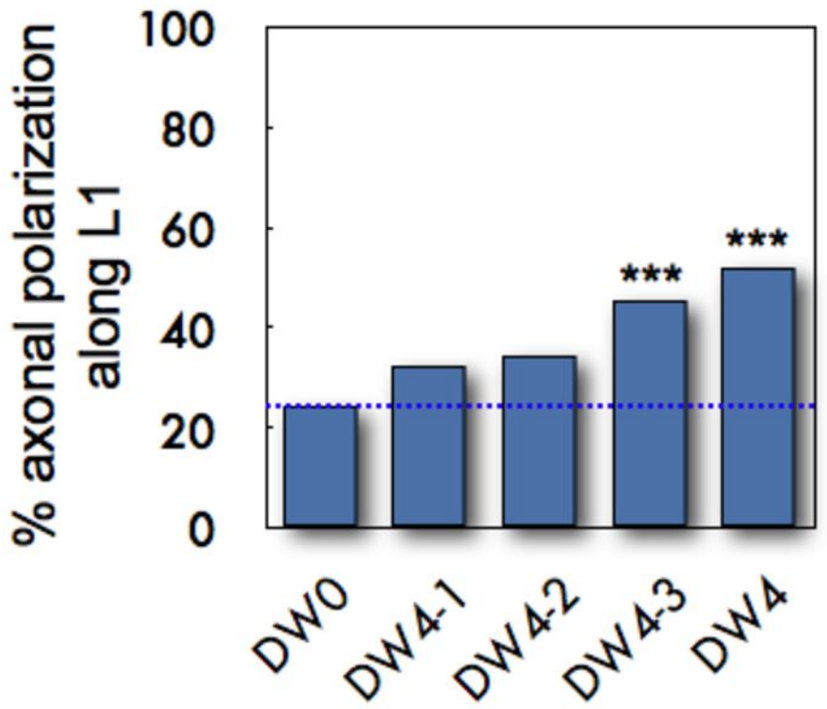

figure-2 (Villard)

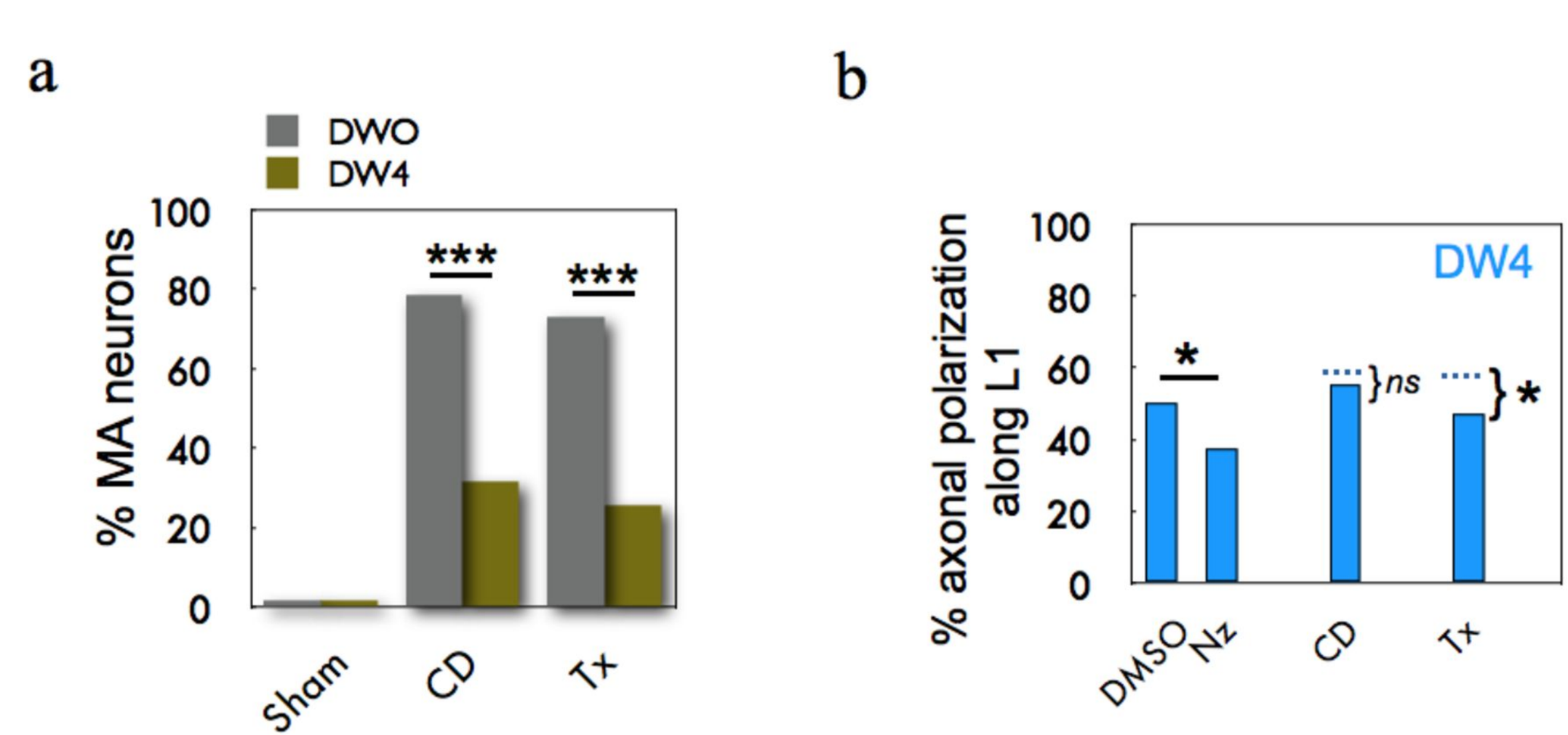

figure-3 (Villard)